

Article

Synthesis of Fuel Grade Molecules from Hydroprocessing of Biomass-Derived Compounds Catalyzed by Magnetic Fe(NiFe)O₄-SiO₂ Nanoparticles

Ahmed Halilu ^{1,2,*} , Tammar Hussein Ali ^{1,3} , Putla Sudarsanam ⁴ and Suresh K. Bhargava ^{5,*} 

¹ Nanotechnology and Catalysis Research Centre (NANOCAT), University of Malaya, Kuala Lumpur 50603, Malaysia; alitamar4@gmail.com

² Department of Petrochemicals and Allied, National Research Institute for Chemical Technology (NARICT), Basawa 1052, Nigeria

³ College of Pharmacy, Al Muthanna University, Al Muthanna, Samawah 66001, Iraq

⁴ Centre for Surface Chemistry and Catalysis, Faculty of Bioscience Engineering, KU Leuven, Celestijnenlaan 200f, 3001 Heverlee, Belgium; sudarsanam.putla@kuleuven.be

⁵ Centre for Advanced Materials and Industrial Chemistry (CAMIC), School of Science, RMIT University, Melbourne 3001, Australia

* Correspondence: ahmed_h@um.edu.my (A.H.); suresh.bhargava@rmit.edu.au (S.K.B.); Tel.: +601128328242 (A.H.); +61-3-99253365 (S.K.B.)

Received: 11 February 2019; Accepted: 28 March 2019; Published: 11 April 2019



Abstract: The development of promising magnetic nanocatalysts is one of the key research topics in the field of catalysis. This is because of their versatile surface physicochemical, magnetic, and size-dependent catalytic properties. Herein, an optimization strategy for the synthesis of high-value fuel grade chemicals from hydro-deoxygenation of biomass-derived furfural and vanillin using a nanostructured magnetic Fe(NiFe)O₄-SiO₂ catalyst, synthesized by a facile one-pot procedure, was presented. Accordingly, effects of calcination temperature from 400, 500, 600 to 700 °C on the structure-activity properties of the magnetic Fe(NiFe)O₄-SiO₂ catalyst was systematically studied. The magnetic Fe(NiFe)O₄-SiO₂ catalyst calcined at 500 °C exhibited the best catalytic performance, giving full conversions of vanillin and furfural, with good selectivity of 63 and 59% to cyclohexane and *n*-pentane (fuel grade chemicals), respectively. The prowess of this catalyst was attributed to its abundant acid properties in addendum to high BET surface area.

Keywords: magnetic nanocatalysts; biomass-derived compounds; hydro-deoxygenation; fuel grade chemicals; structure-activity correlations

1. Introduction

Valorization of lignocellulosic biomass and its derived compounds into fuels and chemicals is a key research topic of the 21st century in view of finding sustainable alternatives to fossil fuel-derived products. Lignocellulosic biomass is abundantly produced via photosynthesis by means of water, sunlight, and atmospheric CO₂. Hence, in addition to providing alternative fuels and chemicals, promising valorization of biomass could assist in reducing the net emissions of CO₂ through the interplay chemistry of biorefinery and photosynthesis processes, which require economically viable processing methods [1–6]. Both homogeneous and heterogeneous catalysts play a critical role in biomass processing towards high-value chemicals. However, efficient catalyst recovery/reusability remains a great challenge, especially in homogeneous catalysis in which both reactants and catalysts are in the same phase, mostly liquid phase. Although filtration or centrifugation are used for the

recovery of heterogeneous catalysts (typically solids), these post-reaction steps are time-consuming, uneconomical, and generates huge amounts of solvent waste. In this context, the application of magnetically recoverable catalysts in biomass valorization would be a promising strategy as they not only enable the efficient catalyst recovery using external magnets, but also exhibit reasonably good catalytic performance because of their unique nanoscale properties [7–13].

Magnetic nanoparticles (MNPs) have been widely used as the catalyst supports as well as the catalytic active components in many chemical reactions, such as oxidation, C–C and C–X (X = N, Cl, S, and O) coupling, and hydroprocessing [14–16]. However, relatively less attention has been paid towards the catalytic application of MNPs in biomass valorization reactions. This is because biomass valorization involves complex reactions, and, thus, understanding the structure–activity properties of MNPs-based catalysts is quite difficult and has not been investigated before. Although structure–activity relationships were proven for non-magnetic nanocatalysts, so far it has been for non-hydroprocessing reactions [17–20]. Therefore, understanding the structure–activity capability of MNPs-based catalysts for the hydrodeoxygenation reaction is necessary, especially for the production of fuel grade molecules from biomass-derived compounds.

In view of the above opportunities, the present work has been focused on modifying the properties of a magnetic Fe(NiFe)O₄-SiO₂ catalyst, synthesized by using a facile one-pot strategy. The effect of calcination temperature from 400 to 700 °C on the magnetic, textural, acid, and catalytic properties of the developed magnetic catalyst was thoroughly investigated. The catalytic efficiency of magnetic Fe(NiFe)O₄-SiO₂ catalysts was tested for hydro-deoxygenation of two biomass-derived compounds, such as furfural (hemicellulose-derived compound) and vanillin (lignin-derived compound). A handful of physicochemical characterization techniques were employed to obtain a clear insight into the textural, acid, and magnetic properties of Fe(NiFe)O₄-SiO₂ catalysts. In this work, we mainly focused on achieving improved yields of saturated hydrocarbons from furfural and vanillin because saturated hydrocarbons can be used as potential fuel grade chemicals. Possible reaction pathways were proposed for the hydro-deoxygenation of furfural and vanillin over the magnetic nanocatalyst.

2. Experimental

2.1. Catalyst Preparation and Heat Treatments

A magnetic Fe(NiFe)O₄-SiO₂ catalyst was prepared similarly to the method reported in the literature [5]. In a typical heat treatment experiment, 2 g of Fe(NiFe)O₄-SiO₂ was placed in a P300 Nabertherm furnace coupled with a temperature controller. Heat treatments were conducted at set point temperature (SPT_n ; $n = 1, 2, 3 \text{ \& } 4$), i.e., $SPT_1 = 400 \text{ }^\circ\text{C}$, $SPT_2 = 500 \text{ }^\circ\text{C}$, $SPT_3 = 600 \text{ }^\circ\text{C}$, and $SPT_4 = 700 \text{ }^\circ\text{C}$ under controlled temperature ramping of 1 °C/min starting from room temperature (RT). During heat treatments, where a $\pm T \text{ }^\circ\text{C}$ error drift was observed from the $RT \sim 28 \text{ }^\circ\text{C}$, the conversion factor $t_1 = T^\circ_{\text{Ramp}} / (SPT_n - RT)$ was used so that 1 °C/min ramping is always maintained for the heat flow across the catalyst material under a static environment ($t_1 = \text{ramping time}$). However, for $RT \neq 28 \text{ }^\circ\text{C}$, SPT_n is inserted together with the $T^\circ_{\text{Ramp}} = 1 \text{ }^\circ\text{C}/\text{min}$ to compute t_1 .

2.2. Catalyst Characterization

N₂ adsorption–desorption studies were carried out for the Fe(NiFe)O₄-SiO₂ catalyst on Micromeritics TriStar II 3020 adsorption apparatus using the ASTM D 3663-03 test method. This was followed by powder X-ray diffraction (XRD) on XRD Bruker D8 advance instrument. High-resolution transmission electron microscopy (HRTEM) analysis of the 400 °C treated Fe(NiFe)O₄-SiO₂ catalyst was also performed on a JEOL JEM-3010. The magnetic properties of Fe(NiFe)O₄-SiO₂ catalysts were measured using a Lakeshore 7400 series vibrating sample magnetometer (VSM), coupled with an electromagnet field sweeping from –10 kOe to +10 kOe at room temperature. The NH₃-TPD analysis of the catalysts was done on TPDRO 1100 series equipped with a TCD detector. The pyridine adsorption FTIR analysis of Fe(NiFe)O₄-SiO₂ catalysts was done on a Bruker FTIR IFS 66/S instrument.

2.3. Catalytic Activity Studies

The catalytic performance of magnetic Fe(NiFe)O₄-SiO₂ nanocatalysts was investigated for the hydro-deoxygenation of furfural and vanillin in an automated 100 mL (42 mm ID) capacity autoclave reactor made of Hast-alloy C 276 material. Activated Fe(NiFe)O₄-SiO₂ catalyst amounting to 60 mg was introduced in 20% (v/v) furfural or 0.3 g vanillin reaction mixture from a catalyst bulb in heptane and heptane:H₂O (95:5) solvents, respectively. The reaction was performed at 250 °C and 90 H₂ bar for 4 h reaction time. After completion of the reaction, an Agilent 6890N with 5973 MSD analyzed the reaction mixture and further quantitative analysis was performed on an Agilent 6890N GC-FID with DB-wax column.

$$\text{Product distribution (\%)} = \frac{n(\text{product})_i}{\sum_{i=j}^m n(\text{detected products})_i} \quad (1)$$

$$\text{Conversion (\%)} = \frac{n(\text{reactant})_{in} - n(\text{reactant})_{out}}{n(\text{reactant})_{in}} \quad (2)$$

$$\text{HDO \%} = \frac{\sum_{i=j}^m wt.(\text{deoxygenated product})_i}{\sum_{i=j}^m wt.(\text{detected products})_i} \quad (3)$$

3. Results and Discussion

3.1. Effect of Temperature on Textural Properties of Fe(NiFe)O₄-SiO₂ Catalyst

Figure 1a shows XRD patterns of magnetic Fe(NiFe)O₄-SiO₂ nanocatalyst treated at various temperatures ranging from 400 °C, 500 °C, 600 °C, and 700 °C. The noticed major reflections at 2θ values represented by 35.64°, 43.49°, 53.81°, 57.32°, and 63.11°, are assigned to Fe₃O₄ phase [21,22]. The average crystallite size of Fe₃O₄, estimated using Scherrer equation [21,22], increased with the increase of heat treatment from 400 to 600 °C and then decreased at 700 °C. The estimated average crystallite sizes for the Fe(NiFe)O₄-SiO₂ catalyst were ~12.55 nm, ~14.53 nm, ~19.80 nm, and ~13.55 nm for 400 °C, 500 °C, 600 °C, and 700 °C heat treatments, respectively. These values, irrespective of the temperature treatment, indicated that all catalysts are still in the super-paramagnetic domain as their crystallite sizes are below 20 nm [23,24]. High-resolution TEM images of the Fe(NiFe)O₄-SiO₂ catalyst calcined at 400 °C are shown in Figure 1b. Magnetic material exhibits crystalline phases and irregularly shaped particles in the nanoscale range (~8–23 nm). The estimated d-spacing (0.297 nm) corresponds to a Fe₃O₄ phase, in line with the XRD results (Figure 1a). N₂ adsorption–desorption isotherms of Fe(NiFe)O₄-SiO₂ catalysts are shown in Figure 1c. The Fe(NiFe)O₄-SiO₂ catalyst treated at 400 °C exhibits type IV isotherm with a H3-type hysteresis loop, revealing the presence of slit-shaped pores (Figure 1c). In contrast, the H1-type hysteresis loop was noticed for 500, 600, and 700 °C treated Fe(NiFe)O₄-SiO₂ catalysts, indicating the formation of well-defined mesopores [25]. The hysteresis loop of Fe(NiFe)O₄-SiO₂ material shifts to higher relative pressures with the increase of heat treatment from 400 to 500 °C and, then, there was no much difference in the shape of the hysteresis loop up to 700 °C. The shifting of the hysteresis loop towards higher relative pressures showed the formation of larger pores in the Fe(NiFe)O₄-SiO₂ catalyst. The BET surface area values were 61.05 m²/g, 57.03 m²/g and 56.5 m²/g for 400 °C, 600 °C, and 700 °C calcined Fe(NiFe)O₄-SiO₂ catalysts, respectively (Figure 1d). However, a superior BET surface area of ~259 m²/g was found for the 500 °C calcined Fe(NiFe)O₄-SiO₂ catalyst [5]. This suggested that the specific surface area was maximized for 500 °C calcined sample in order to compensate for surface atom energetics in contrast to 400, 600, and 700 °C calcined samples. Their BET surface areas were minimized to compensate for surface atom energetics. The pore volume and pore size of Fe(NiFe)O₄-SiO₂ catalysts were found to be in the range of 0.21–0.9 cm³/g and 6.8–10.9 nm, respectively (Figure 1d).

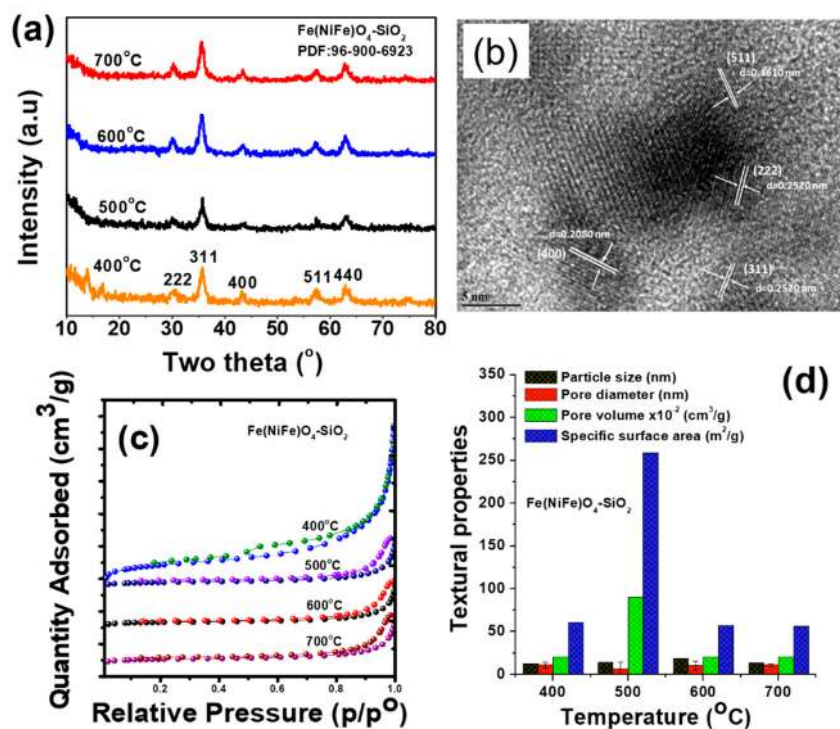


Figure 1. Physicochemical properties of $\text{Fe}(\text{NiFe})\text{O}_4\text{-SiO}_2$ catalysts: (a) powder XRD patterns, (b) TEM image of $\text{Fe}(\text{NiFe})\text{O}_4\text{-SiO}_2$ calcined at 400 °C, (c) N_2 adsorption–desorption isotherms, and (d) textural properties.

3.2. Effect of Calcination Temperature on Acid Properties of $\text{Fe}(\text{NiFe})\text{O}_4\text{-SiO}_2$ Catalysts

Figure 2 shows NH_3 -TPD and pyridine FT-IR profiles of $\text{Fe}(\text{NiFe})\text{O}_4\text{-SiO}_2$ magnetic catalysts. According to Figure 2a, the temperature at which NH_3 molecules are desorbed from the catalyst surface reveals the acid strength of the catalysts. Generally, the peaks that was observed at <200 °C, 300–500 °C range and >500 °C can be assigned to NH_3 molecules desorbed from surface weak, medium, and strong acid sites, respectively [25]. A higher intensity peak corresponding to strong acid sites was noticed at 554, 556, 552, and 554 °C for the $\text{Fe}(\text{NiFe})\text{O}_4\text{-SiO}_2$ catalyst calcined at 400, 500, 600, and 700 °C, respectively (Figure 2a). Medium strength acid site peaks were noticed at 487, 485, 487, and 489 °C for the same range of temperature treatments (Figure 2a). Weak acid site peaks were also noticed at 152, 158, 146, and 142 °C for the same range of temperature treatments. These observations indicated that irrespective of the temperature treatment within the range of 400 °C to 700 °C, the catalyst contains weak, medium and strong acid sites on its surface. Additionally, pyridine adsorbed FT-IR studies reveal the presence of both Brönsted and Lewis acid sites on the catalyst surface (Figure 2b). The $\text{Fe}(\text{NiFe})\text{O}_4\text{-SiO}_2$ catalyst calcined at 700 °C exhibited several peaks due to strong Lewis acidic site-bonded pyridine at 1437 cm^{-1} , weak Lewis acidic site-bonded pyridine at 1580 cm^{-1} and pyridinium ion on Brönsted acid sites at 1645 cm^{-1} as well as trivial peaks due to hydrogen bonded pyridine at 1597 cm^{-1} . For the catalyst calcined at 600 °C, very low-intensity peaks were observed, corresponding to strong Lewis acidic site-bonded pyridine at 1439 cm^{-1} and pyridinium ion on Brönsted acidic sites at 1655 cm^{-1} . The peak at 1482 cm^{-1} can be assigned to pyridine associated with both Brönsted and Lewis acid sites, whereas the peak at 1581 cm^{-1} is assigned to weak Lewis acidic site-bonded pyridine and the peak at 1437 cm^{-1} corresponds to strong Lewis acidic site-bonded pyridine for $\text{Fe}(\text{NiFe})\text{O}_4\text{-SiO}_2$ (calcined at 500 °C). The catalyst calcined at 400 °C exhibited very low-intensity peaks at 1439 cm^{-1} for strong Lewis acidic site-bonded pyridine and 1655 cm^{-1} for pyridinium ion on Brönsted acid sites. These observations are in line with previous reports [26–28]. Therefore, the developed magnetic catalysts exhibited considerable amounts of all types of acidic sites,

which could play a key role in hydrodeoxygenation of biomass-derived compounds as discussed in the catalytic activity part.

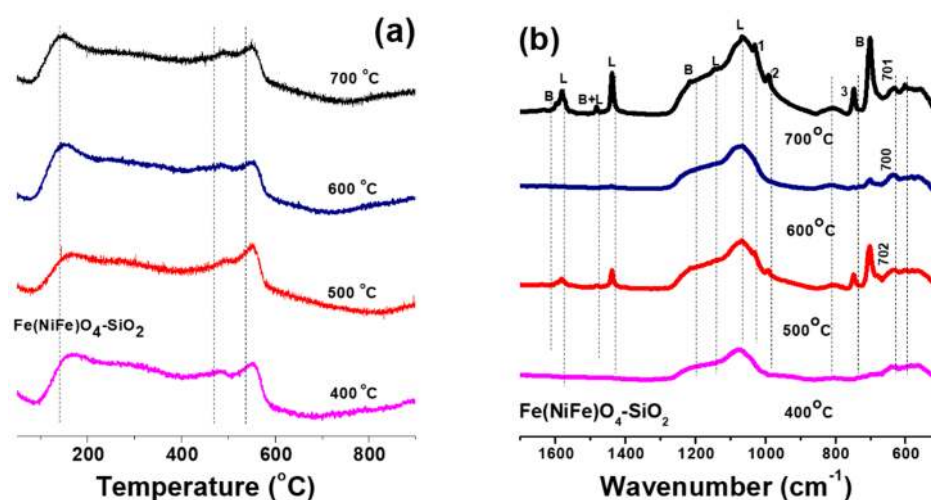


Figure 2. Surface acidity analysis of $\text{Fe}(\text{NiFe})\text{O}_4\text{-SiO}_2$ catalysts: (a) NH_3 -TPD profiles and (b) pyridine adsorption FT-IR profiles.

3.3. Effect of Calcination Temperature on Magnetic Properties of $\text{Fe}(\text{NiFe})\text{O}_4\text{-SiO}_2$ Catalyst

The correlation of magnetic properties (magnetization, magnetic remanence, and coercivity) of $\text{Fe}(\text{NiFe})\text{O}_4\text{-SiO}_2$ catalysts with the calcination temperature is shown in Figure 3. Therein, the results revealed that all the $\text{Fe}(\text{NiFe})\text{O}_4\text{-SiO}_2$ catalysts exhibit considerable magnetization: 35.11 emu/g (700 °C), 32.75 emu/g (600 °C), 38.65 emu/g (500 °C), and 32.91 emu/g (400 °C), supporting their promising applications for facile catalyst recovery. On the other hand, lower coercivity and remanence values were found in the $\text{Fe}(\text{NiFe})\text{O}_4\text{-SiO}_2$ catalyst at all heat treatments in comparison to the magnetization.

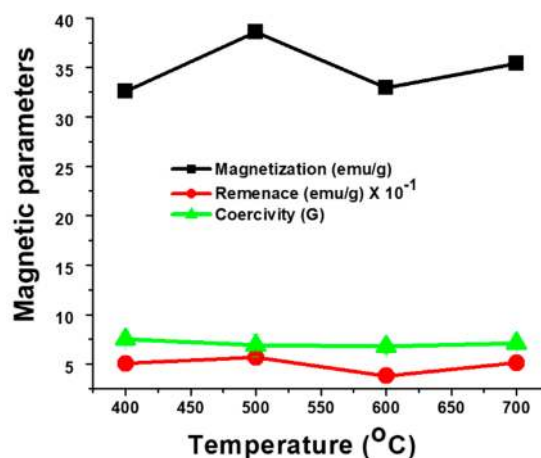


Figure 3. Distribution of magnetic parameters (magnetization, magnetic remanence, and coercivity) for $\text{Fe}(\text{NiFe})\text{O}_4\text{-SiO}_2$ catalysts.

3.4. Activity Studies of Magnetic $\text{Fe}(\text{NiFe})\text{O}_4\text{-SiO}_2$ Catalyst

3.4.1. Hydrodeoxygenation of Vanillin

The catalytic efficiency of heat-treated magnetic $\text{Fe}(\text{NiFe})\text{O}_4\text{-SiO}_2$ catalysts was studied for hydrodeoxygenation (HDO) of vanillin and furfural at 250 °C and 90 H_2 bar for 4 h. The main products in the HDO of vanillin were cyclohexane, cyclohexanol, cyclohexanone, phenol, 2-methoxyphenol, and 3-(hydroxymethyl)-2-methoxyphenol (Table 1). Vanillin conversion was found to be 100% for all

the calcined catalysts. In contrast, calcination temperature showed a noticeable effect on the catalyst's performance in product selectivity. For the $\text{Fe}(\text{NiFe})\text{O}_4\text{-SiO}_2$ (400 °C) catalyst, a high selectivity of vanillin HDO to cyclohexanone (~56%) was established, whereas only a 21% cyclohexane selectivity was achieved. Similarly, the catalyst treated at a higher temperature showed low selectivity to cyclohexanone, while the selectivity of cyclohexane was increased: $\text{Fe}(\text{NiFe})\text{O}_4\text{-SiO}_2$ (500 °C) = 63%, $\text{Fe}(\text{NiFe})\text{O}_4\text{-SiO}_2$ (600 °C) = 54%, and $\text{Fe}(\text{NiFe})\text{O}_4\text{-SiO}_2$ (700 °C) = 53%. In addition, considerable amounts of cyclohexanol and 2-methoxyphenol are formed over the $\text{Fe}(\text{NiFe})\text{O}_4\text{-SiO}_2$ catalyst at all calcination temperatures. Despite the calcination temperature applied, negligible amounts of phenol and 3-(hydroxymethyl)-2-methoxyphenol were observed. In $\text{Fe}(\text{NiFe})\text{O}_4\text{-SiO}_2$ (500 °C) the catalyst showed high selectivity to cyclohexane (Table 1). These results are in accordance to the explanation given in Sections 3.4.2 and 3.5 and to the fact that acidity and different acid sites of the catalyst can improve the cracking steps through dehydration, in line with the literature reports [29,30]. In addition, the catalyst calcined at 500 °C showed good reusability for at least four cycles (Figure 4).

Table 1. Product distribution in HDO of vanillin over $\text{Fe}(\text{NiFe})\text{O}_4\text{-SiO}_2$ catalysts at 250 °C and 90 bar H_2 for 4 h.

Catalyst	Vanillin Conversion (%)	Selectivity (%)						% HDO
								
$\text{Fe}(\text{NiFe})\text{O}_4\text{-SiO}_2$ (400 °C)	100	56	21	2	4	-	17	17.89
$\text{Fe}(\text{NiFe})\text{O}_4\text{-SiO}_2$ (500 °C)	100	14	63	-	5	10	8	20.20
$\text{Fe}(\text{NiFe})\text{O}_4\text{-SiO}_2$ (600 °C)	100	5	54	-	2	20	19	20.08
$\text{Fe}(\text{NiFe})\text{O}_4\text{-SiO}_2$ (700 °C)	100	4	53	-	1	33	9	19.51

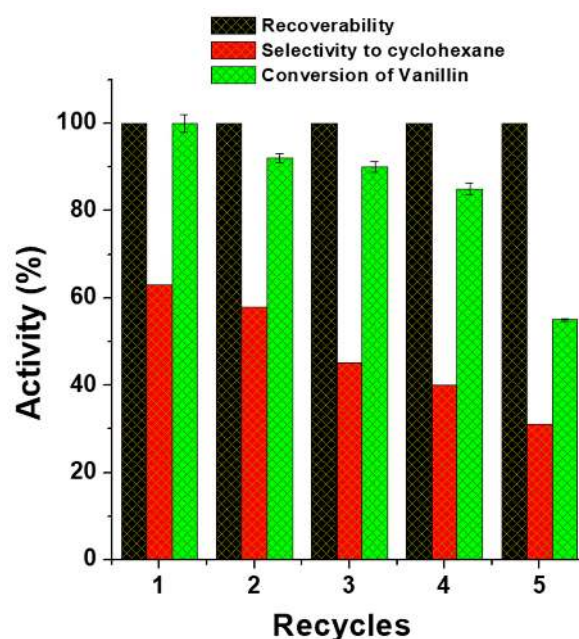


Figure 4. Recovery and reusability of $\text{Fe}(\text{NiFe})\text{O}_4\text{-SiO}_2$ catalysts calcined at 500 °C in hydrodeoxygenation of vanillin at 250 °C and 90 bar H_2 for 4 h.

3.4.2. Hydrodeoxygenation of Furfural

Furfural hydrodeoxygenation results reveal (Table 2) that the calcination temperature has a negligible influence towards furfural conversion. The furfural conversion was found to be 100% for all the catalysts. Three products, namely furfuryl alcohol, tetrahydrofuran, and n-pentane were formed in this reaction. The performance of magnetic catalysts and the effect of calcination temperature in

hydrodeoxygenation of furfural are evaluated based on the selectivity of saturated hydrocarbon, i.e., n-pentane, which does not have any oxygen-containing groups. Among the products formed, very low selectivity of furfuryl alcohol was achieved for all the catalysts. The Fe(NiFe)O₄-SiO₂ (700 °C) shows a high selectivity of tetrahydrofuran, i.e., 58%. Among the catalysts tested, Fe(NiFe)O₄-SiO₂ (500 °C) catalyst showed 100% furfural conversion and 59% n-pentane selectivity. Hydrodeoxygenation is a typical acid-site driven reaction in which acid sites initiate the removal of oxygen via dehydration and the hydrogenation step is promoted by active phase Ni metal sites. It was obvious that Fe(NiFe)O₄-SiO₂ (500 °C) showed the best catalytic performance in the HDO of furfural and vanillin. As shown in Figure 2, despite the calcination temperature employed, the Fe(NiFe)O₄-SiO₂ catalyst exhibited a high-intensity peak at around 550 °C, indicating the presence of more number of strong acid sites. In addition, the Fe(NiFe)O₄-SiO₂ catalyst calcined at 500 °C showed superior BET surface area of ~259 m²/g compared to all the other catalysts. The catalytic materials with a high BET surface area can contain uniform dispersion of catalytic active phase species. Therefore, the high catalytic performance of the Fe(NiFe)O₄-SiO₂ catalyst calcined at 500 °C is likely to be due to the synergistic effect of its acid properties and larger BET surface area. Moreover, the catalyst calcined at 500 °C showed good reusability up to five cycles as shown in Figure 5.

Table 2. Products distribution in hydrodeoxygenation of furfural over Fe(NiFe)O₄-SiO₂ catalysts, conducted at 250 °C and 90 bar H₂ for 4 h.

Catalyst	Furfural Conversion (%)	Selectivity (%)			% HDO
					
Fe(NiFe)O ₄ -SiO ₂ (400 °C)	100	12	42	46	29.78
Fe(NiFe)O ₄ -SiO ₂ (500 °C)	100	8	33	59	29.78
Fe(NiFe)O ₄ -SiO ₂ (600 °C)	100	13	34	53	29.78
Fe(NiFe)O ₄ -SiO ₂ (700 °C)	100	8	58	34	29.78

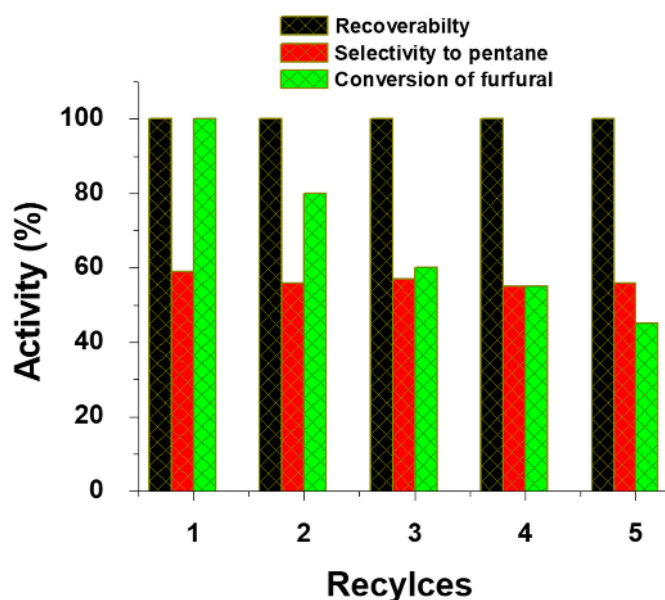
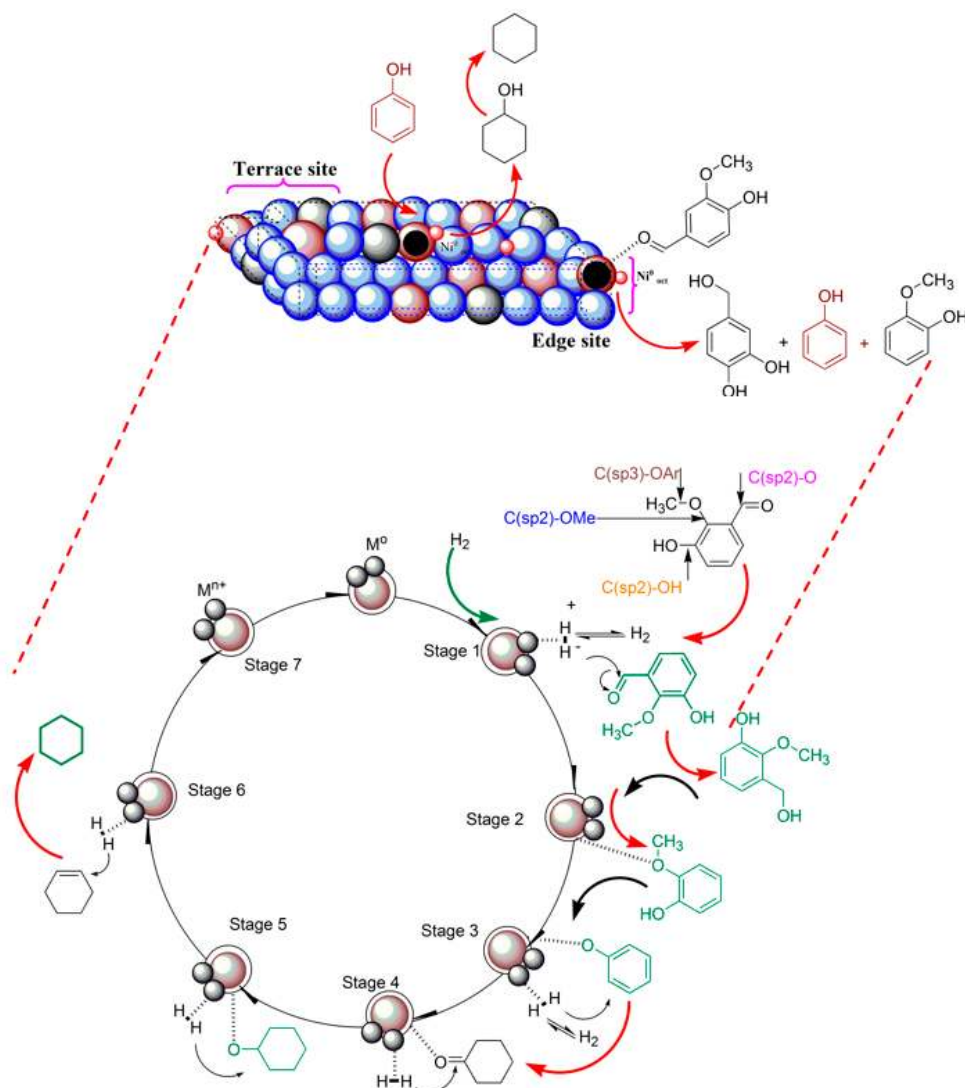


Figure 5. Recovery and reusability of the Fe(NiFe)O₄-SiO₂ catalyst calcined at 500 °C in hydrodeoxygenation of furfural at 250 °C and 90 bar H₂ for 4 h.

3.5. Possible Reaction Pathways

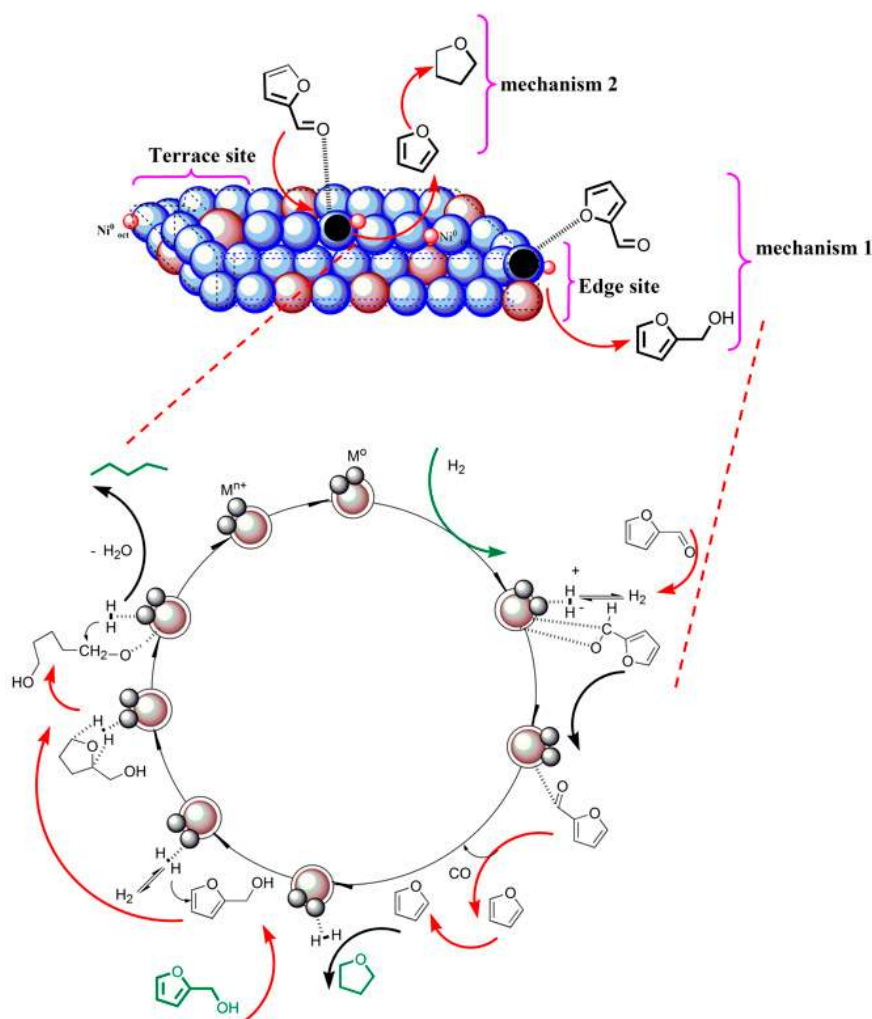
Scheme 1 and 2 show the possible reaction pathways for the HDO of vanillin and furfural at 250 °C and 90 bar H₂, respectively. The active metal Ni and acid properties of Fe(NiFe)O₄-SiO₂ catalysts could play a key role in the production of fuel grade chemicals from the HDO of vanillin and

furfural. As shown in Scheme 1, transformation of vanillin can be initiated with four potential C-O bonds having different bond dissociation energies (BDEs): $C(sp^3)-OAr$ (~262–276 kJ/mol), $C(sp^2)-OMe$ (~409–421 kJ/mol), $C(sp^2)-OH$ (~466 kJ/mol), and $C(sp^2)-O$ (~732 kJ/mol). As shown earlier, the magnetic $Fe(NiFe)O_4-SiO_2$ catalyst surface can possess non-hydrogen spillover attributes [5]. Therefore, on the basis of BDEs over the catalyst surface, bond cleavage likely follows the order during vanillin HDO: $C(sp^3)-OAr < C(sp^2)-OMe < C(sp^2)-OH < C(sp^2)-O$. Most probably, the bond cleavage of vanillin will follow the direct C–O cleavage with the attack of hydrogen at the ipso position (–OH) and at the meso (–OCH₃) position followed by hydrogenation on the metal site at the ortho position and then dehydration step over acid sites. This reaction pathway is initiated by tautomerization (Scheme 1). Accordingly, the cyclohexane is formed through a series of reactions from vanillin. By implication, phenol is transformed to phenoxide ion in the presence of acid sites. The phenoxide species can diffuse towards the Ni metal active phase to attack electrophiles, such as H^+ obtained from the dissociation of H_2 over the metal active phase in the $Fe(NiFe)O_4-SiO_2$ catalyst, giving cyclohexanone product [31]. In continuation, cyclohexanone is then directly hydrogenated to form cyclohexanol. The magnetic attributes of the catalysts then induce electron mobility that can enhance the adsorption of cyclohexanol on the catalyst acid sites at the OH terminal, giving cyclohexene through dehydration step. Finally, the cyclohexene is hydrogenated to yield cyclohexane.



Scheme 1. Possible reaction pathway for HDO of vanillin over $Fe(NiFe)O_4-SiO_2$ catalysts.

As observed in the HDO of vanillin, similar trends are also possible for the HDO of furfural by considering the fact that the electron density distribution around the carbonyl functionality stimulates the furfural molecules for hydrogen attack and subsequent decarbonylation at 250 °C and 90 bar H_2 conditions. As shown in Scheme 2, adsorption and reaction steps initiating the formation of tetrahydrofuran from furfural was due to the presence of adequate acidic sites, active metal phase, and magnetic functions of the catalysts. The formed tetrahydrofuran is directly hydrogenated over the metal active phase in $Fe(NiFe)O_4-SiO_2$ catalyst, giving furfuryl alcohol. Finally, pentane is formed via the ring opening of furfuryl alcohol and the subsequent dehydration step.



Scheme 2. Possible reaction pathway for hydro-deoxygenation of furfural over $Fe(NiFe)O_4-SiO_2$ catalysts.

4. Conclusions

This study rationalized a systematic heat treatment of a magnetic $Fe(NiFe)O_4-SiO_2$ catalyst for vanillin and furfural HDO to produce fuel grade chemicals. The magnetic $Fe(NiFe)O_4-SiO_2$ catalyst is suitable for hydrodeoxygenation reactions due to the presence of optimized amounts of metal (Ni) and acid active sites. The 500 °C was found to be a suitable calcination temperature for treating the $Fe(NiFe)O_4-SiO_2$ catalyst for hydro-processing reactions, evidenced from the selectivity of 63% cyclohexane and 59% n-pentane fuel grade hydrocarbons from HDO of vanillin and furfural at 250 °C and 90 H_2 bar for 4 h, respectively. The catalytic efficiency of $Fe(NiFe)O_4-SiO_2$ (500 °C) was due to the optimized acid sites, superior surface area, and unique magnetization property.

Author Contributions: A.H. has conducted the experiments and the manuscript was written through the contribution of all authors.

Funding: This work was supported by the High Impact Research (HIR) grant number F-00032, Universiti Malaya (UM) and the National Research Institute for Chemical Technology (NARICT), Nigeria through the collaboration on renewable energy.

Acknowledgments: The authors dedicate this study to Late Sharifah Bee Abd Hamid, the founder of Nanotechnology and Catalysis Research Center (NANOCAT), Malaysia. The authors also appreciate the initiative of Idris M. Bugaje on the collaboration with NANOCAT.

Conflicts of Interest: The authors declare no conflicts of interest.

References

1. Halilu, A. Is there a realistic solution to upgrading bio-oil to fuel and chemicals? *Inform* **2017**, *28*, 22–24. [[CrossRef](#)]
2. Sudarsanam, P.; Zhong, R.; van den Bosch, S.; Coman, S.M.; Parvulescu, V.I.; Sels, B.F. Functionalised heterogeneous catalysts for sustainable biomass valorisation. *Chem. Soc. Rev.* **2018**, *47*, 8349–8402. [[CrossRef](#)]
3. Ambursa, M.M.; Sudarsanam, P.; Voon, L.H.; Hamid, S.B.A.; Bhargava, S.K. Bimetallic Cu-Ni catalysts supported on MCM-41 and Ti-MCM-41 porous materials for hydrodeoxygenation of lignin model compound into transportation fuels. *Fuel Process. Technol.* **2017**, *162*, 87–97. [[CrossRef](#)]
4. Ambursa, M.M.; Ali, T.H.; Lee, H.V.; Sudarsanam, P.; Bhargava, S.K.; Hamid, S.B.A. Hydrodeoxygenation of dibenzofuran to bicyclic hydrocarbons using bimetallic Cu–Ni catalysts supported on metal oxides. *Fuel* **2016**, *180*, 767–776. [[CrossRef](#)]
5. Halilu, A.; Ali, T.H.; Atta, A.Y.; Sudarsanam, P.; Bhargava, S.K.; Hamid, S.B.A. Highly Selective Hydrogenation of Biomass-Derived Furfural into Furfuryl Alcohol Using a Novel Magnetic Nanoparticles Catalyst. *Energy Fuels* **2016**, *30*, 2216–2226. [[CrossRef](#)]
6. Sudarsanam, P.; Peeters, E.; Makshina, E.V.; Parvulescu, V.I.; Sels, B.F. Advances in porous and nanoscale catalysts for viable biomass conversion. *Chem. Soc. Rev.* **2019**. [[CrossRef](#)] [[PubMed](#)]
7. Polshettiwar, V.; Luque, R.; Fihri, A.; Zhu, H.; Bouhrara, M.; Basset, J.-M. Magnetically recoverable nanocatalysts. *Chem. Rev.* **2011**, *111*, 3036–3075. [[CrossRef](#)] [[PubMed](#)]
8. Zhang, L.; Li, P.; Li, H.; Wang, L. A recyclable magnetic nanoparticles supported palladium catalyst for the Hiyama reaction of aryltrialkoxysilanes with aryl halides. *Catal. Sci. Tech.* **2012**, *2*, 1859–1864. [[CrossRef](#)]
9. Gawande, M.B.; Branco, P.S.; Varma, R.S. Nano-magnetite (Fe₃O₄) as a support for recyclable catalysts in the development of sustainable methodologies. *Chem. Soc. Rev.* **2013**, *42*, 3371–3393. [[CrossRef](#)] [[PubMed](#)]
10. Wang, D.; Astruc, D. Fast-Growing Field of Magnetically Recyclable Nanocatalysts. *Chem. Rev.* **2014**, *114*, 6949–6985. [[CrossRef](#)]
11. Sharma, R.K.; Dutta, S.; Sharma, S.; Zboril, R.; Varma, R.S.; Gawande, M.B. Fe₃O₄ (iron oxide)-supported nanocatalysts: Synthesis, characterization and applications in coupling reactions. *Green Chem.* **2016**, *18*, 3184–3209. [[CrossRef](#)]
12. Gawande, M.B.; Monga, Y.; Zboril, R.; Sharma, R.K. Silica-decorated magnetic nanocomposites for catalytic applications. *Coord. Chem. Rev.* **2015**, *288*, 118–143. [[CrossRef](#)]
13. Gawande, M.B.; Rathi, A.K.; Branco, P.S.; Nogueira, I.D.; Velhinho, A.; Shrikhande, J.J.; Indulkar, U.U.; Jayaram, R.V.; Ghumman, C.A.A.; Bundaleski, N.; et al. Regio- and Chemoselective Reduction of Nitroarenes and Carbonyl Compounds over Recyclable Magnetic Ferrite–Nickel Nanoparticles (Fe₃O₄–Ni) by Using Glycerol as a Hydrogen Source. *Chem. Eur. J.* **2012**, *18*, 12628–12632. [[CrossRef](#)] [[PubMed](#)]
14. Baig, R.B.N.; Varma, R.S. Magnetically retrievable catalysts for organic synthesis. *Chem. Commun.* **2013**, *49*, 752–770. [[CrossRef](#)] [[PubMed](#)]
15. Sobhani, S.; Ramezani, Z. Synthesis of arylphosphonates catalyzed by Pd-imino-Py-[gamma]-Fe₂O₃ as a new magnetically recyclable heterogeneous catalyst in pure water without requiring any additive. *RSC Adv.* **2016**, *6*, 29237–29244. [[CrossRef](#)]
16. Hamid, S.B.A.; Halilu, A.; Gbadamasi, S.; Hakim, L. Opportunities in Utilization of Lignocellulosic Biomass Oil to Bio-Esters. In *Renewable Energy and Sustainable Developments*; Al-Douri, Y., Ed.; Scientific & Academic Publishing: Rosemead, CA, USA, 2014.

17. Amin, M.H.; Putla, S.; Hamid, S.B.A.; Bhargava, S.K. Understanding the role of lanthanide promoters on the structure–activity of nanosized Ni/ γ -Al₂O₃ catalysts in carbon dioxide reforming of methane. *Appl. Catal. A* **2015**, *492*, 160–168. [[CrossRef](#)]
18. Otake, K.-i.; Cui, Y.; Buru, C.T.; Li, Z.; Hupp, J.T.; Farha, O.K. Single-Atom-Based Vanadium Oxide Catalysts Supported on Metal–Organic Frameworks: Selective Alcohol Oxidation and Structure–Activity Relationship. *J. Am. Chem. Soc.* **2018**, *140*, 8652–8656. [[CrossRef](#)] [[PubMed](#)]
19. Sachs, M.; Sprick, R.S.; Pearce, D.; Hillman, S.A.; Monti, A.; Guilbert, A.A.; Brownbill, N.J.; Dimitrov, S.; Shi, X.; Blanc, F. Understanding structure-activity relationships in linear polymer photocatalysts for hydrogen evolution. *Nat. Commun.* **2018**, *9*, 4968. [[CrossRef](#)]
20. Hillary, B.; Sudarsanam, P.; Amin, M.H.; Bhargava, S.K. Nanoscale Cobalt–Manganese Oxide Catalyst Supported on Shape–Controlled Cerium Oxide: Effect of Nanointerface Configuration on Structural, Redox, and Catalytic Properties. *Langmuir* **2017**, *33*, 1743–1750. [[CrossRef](#)] [[PubMed](#)]
21. Sudarsanam, P.; Hillary, B.; Mallesham, B.; Rao, B.G.; Amin, M.H.; Nafady, A.; Alsalmeh, A.M.; Reddy, B.M.; Bhargava, S.K. Designing CuOx Nanoparticle-Decorated CeO₂ Nanocubes for Catalytic Soot Oxidation: Role of the Nanointerface in the Catalytic Performance of Heterostructured Nanomaterials. *Langmuir* **2016**, *32*, 2208–2215. [[CrossRef](#)]
22. Sudarsanam, P.; Hillary, B.; Amin, M.H.; Hamid, S.B.A.; Bhargava, S.K. Structure-activity relationships of nanoscale MnO_x/CeO₂ heterostructured catalysts for selective oxidation of amines under eco-friendly conditions. *Appl. Catal. B Environ.* **2016**, *185*, 213–224. [[CrossRef](#)]
23. Tenzer, R. Influence of particle size on the coercive force of barium ferrite powders. *J. Appl. Phys.* **1963**, *34*, 1267–1268. [[CrossRef](#)]
24. Sjögren, C.E.; Johansson, C.; Nævestad, A.; Sontum, P.C.; Briley-Sæbø, K.; Fahlvik, A.K. Crystal size and properties of superparamagnetic iron oxide (SPIO) particles. *Magn. Reson. Imaging* **1997**, *15*, 55–67. [[CrossRef](#)]
25. Mistura, G.; Pozzato, A.; Greci, G.; Bruschi, L.; Tormen, M. Continuous adsorption in highly ordered porous matrices made by nanolithography. *Nat. Commun.* **2013**, *4*, 2966. [[CrossRef](#)] [[PubMed](#)]
26. Farneth, W.; Gorte, R. Methods for characterizing zeolite acidity. *Chem. Rev.* **1995**, *95*, 615–635. [[CrossRef](#)]
27. Hutchings, G.J.; Lee, D.F. Control of product selectivity for the epoxidation of allyl alcohol by variation of the acidity of the catalyst TS-1. *Chem. Commun.* **1994**, *9*, 1095–1096. [[CrossRef](#)]
28. Sumiya, S.; Oumi, Y.; Uozumi, T.; Sano, T. Characterization of AISBA-15 prepared by post-synthesisaluminum with trimethylaluminum. *J. Mater. Chem.* **2001**, *11*, 1111–1115. [[CrossRef](#)]
29. Rana, M.S.; Srinivas, B.N.; Maity, S.K.; Dhar, G.M.; Rao, T.S.R.P. Origin of Cracking Functionality of Sulfided (Ni) CoMo/SiO₂–ZrO₂ Catalysts. *J. Catal.* **2000**, *195*, 31–37. [[CrossRef](#)]
30. Xinghua, Z.; Tiejun, W.; Longlong, M.; Chuangzhi, W. Aqueous-phase catalytic process for production of pentane from furfural over nickel-based catalysts. *Fuel* **2010**, *89*, 2697–2702. [[CrossRef](#)]
31. Mortensen, P.M.; Grunwaldt, J.-D.; Jensen, P.A.; Jensen, A.D. Screening of Catalysts for Hydrodeoxygenation of Phenol as a Model Compound for Bio-oil. *ACS Catal.* **2013**, *3*, 1774–1785. [[CrossRef](#)]

